THE UNIVERSITY *of* EDINBURGH
School of Physics
and Astronomy

Terahertz Methods for Material Characterisation

Harrison F. Squires[1]

School of Physics and Astronomy, University of Edinburgh, Edinburgh, UK

(Dated: January 3, 2026)

The following review introduces and discusses both free-space and transmission line methods for characterising materials using terahertz (THz) frequencies. Initially, terahertz time-domain spectroscopy (THz-TDS) is introduced, and its underlying mechanism and merits are described. Selected industrial applications are presented, along with suggestions for future research directions. Next, ellipsometry is introduced, detailing the advantages it presents with respect to sample geometry. A vector network analyser (VNA)-based approach is then introduced as the key transmission line method. A quasi-free-space method, using a VNA and a material characterisation kit (MCK), is also presented. Fourier Transform Infrared (FTIR) spectroscopy is then discussed, notable for its broad spectral coverage. Finally, an inter-comparison is performed, and a flowchart is devised to indicate when each technique is most appropriate.

ACRONYMS

AsLS: Asymmetric Least Squares. 5

CNN: Convolution Neural Network. 4, 10

DFT: Density Functional Theory. 2

DNR: Dynamic Range. 3, 12

FS: Free-Space. 1, 2, 5, 7–10, 12

FSS: Frequency Selective Surfaces. 8, 10

FTIR: Fourier Transform Infrared. 1, 7–10, 12

MCK: Material Characterisation Kit. 7, 8, 10

NRW: Nicholson, Ross and Weir. 6, 7

PCA: Photoconductive Antenna. 2–4, 8

SNR: Signal-to-Noise Ratio. 3, 4, 9, 12

THz: Terahertz. 1–3, 6, 7, 11

THz-TDS: Terahertz Time Domain Spectroscopy. 1–10, 12

TL: Transmission Line. 1, 4, 6–10

TRL: Through-Reflect-Line. 6, 8, 10

VNA: Vector Network Analyser. 1, 2, 4–10, 12

WR: Waveguide Rectangular. 7

I. INTRODUCTION

Terahertz methods for material characterisation refer to methods which utilise electromagnetic radiation in the frequency range of 0.2 THz to 10 THz[1,2]. There are two broad categories of methods used in academic and industry settings: Free-Space (FS) and Transmission Line (TL) based methods. FS methods typically refer to Terahertz Time Domain Spectroscopy (THz-TDS)[1]; although other FS methods exist, such as a FS-Vector Network Analyser (VNA) configurations and Fourier Transform Infrared (FTIR)[3,4]. TL refers to wave propagation through a guided medium rather than through FS. The motivation behind using Terahertz (THz) is that it enables the measurement of both the real and imaginary (complex) components of various important quantities, such as the refractive index $\tilde{n}$, dielectric constant $\tilde{\varepsilon}$, and magnetic permeability $\tilde{\mu}$, without the need for analytical methods such as Kramers–Kronig[5]:

$$\left(\mathrm{Re}\left(\varepsilon[\omega]\right) = 1 + \frac{2}{\pi}\mathcal{P}\int_{-\infty}^{\infty}\frac{\omega'\ \mathrm{Im}\left(\varepsilon[\omega']\right)}{\omega'^2-\omega^2}\,d\omega'\right).$$

More explicitly, by using THz-based methods for material characterisation it is possible to simultaneously mea-

sure both magnitude information and phase information of some particular material. This is because, using THz-TDS, we can obtain a measurement of the electric field within a material itself, not just the intensity $|E_{\mathrm{THz}}|^2$ which requires Kramers-Kronig to analytically calculate phase. Similarly, from a VNA, we obtain S-parameters, and from these, phase information is retained intrinsically, so further analytical techniques are not required[2].

This is desirable since Kramers-Kronig requires spectral information of frequencies from $\omega = 0$ (DC) $\rightarrow \omega = \infty$, clearly lifting this limitation is advantageous[1].

Contextually, this has a wide-range of applications in the detection of drugs and explosives without the need for physically penetrating the packaging. There is also a host of pharmacological and biological promise for the technology that is being actively researched[5].

II. FROM $\tilde{\varepsilon}$ AND $\tilde{\mu}$ TO MATERIAL PROPERTIES

Before reviewing specific measurement techniques, it is useful to summarise the key material parameters derivable from THz measurements and the relationships between them. These definitions will be used throughout the subsequent sections.

II.A. Non-Magnetic Materials ($\tilde{\mu} \approx 1$)

For the vast majority of dielectrics, the magnetic permeability is unitary, meaning that $\tilde{n}^2 \approx \tilde{\varepsilon}$. In this case, $\tilde{\varepsilon}$ can be used alone to derive a number of quantities of potential interest:

- **Refractive index:** $n = \mathrm{Re}\left(\sqrt{\tilde{\varepsilon}}\right)$, describing wave propagation speed.
- **Extinction coefficient:** $\kappa = \mathrm{Im}\left(\sqrt{\tilde{\varepsilon}}\right)$, related to attenuation.
- **Absorption coefficient:** $\alpha = \frac{4\pi\kappa}{\lambda}$, describing exponential decay of the E-field amplitude.
- **Loss tangent:** $\tan\delta = \frac{\mathrm{Im}(\varepsilon)}{\mathrm{Re}(\varepsilon)}$, commonly used to quantify dielectric loss.

These quantities are often reported in place of $\tilde{\varepsilon}$ directly, as they more clearly relate to physical observables like transmission spectra, reflection, and power loss.

II.B. Magnetic Materials ($\tilde{\mu} \neq 1$)

For magnetic materials, the assumption $\tilde{\mu} \approx 1$ no longer holds. In this case, the full complex refractive index becomes:

$$\tilde{n} = \sqrt{\tilde{\varepsilon}\tilde{\mu}}.$$

This makes it necessary to measure both $\tilde{\varepsilon}$ and $\tilde{\mu}$ to accurately determine the following parameters:

- **Magnetic loss tangent:** $\tan\delta_\mu = \frac{\mathrm{Im}(\mu)}{\mathrm{Re}(\mu)}$, quantifying magnetic loss in a material.
- **(Absolute) Impedance:** $Z = \sqrt{\frac{\tilde{\mu}}{\tilde{\varepsilon}}}$, relevant for wave reflection and matching.

Accurate characterisation of magnetic response important for any magnetic material exhibiting a non-unitary permeability. Including THz metamaterials, where resonant magnetic behaviour is deliberately engineered.

III. BROAD OVERVIEW OF FREE-SPACE THZ-TDS

III.A. Non-magnetic materials ($\mu \approx 1$)

Section largely summarised from Neu and Schmuttenmaer[1]

The most prominent FS method to characterise materials is THz-TDS. It can be used to identify chemical components, and is often paired with Density Functional Theory (DFT) to probe investigations into the identification of drugs and explosives[6]. Furthermore, it has been used to validate the homogeneity and uniformity of graphene, a growing material of interest and in the study of paint coatings, skin cancer and more. This is a spectroscopy-based method, that is we are interested in the energy of photons in the sample. Typically, Photoconductive Antenna (PCA) is used for the generation a THz pulse.

A femtosecond pump laser[6](e.g. Ti:Sapphire laser) is directed towards a semiconductor (e.g. low-temperature-grown GaAs mounted on a GaAs substrate) whose bandgap matches the photon energy of the laser, such that electrons can be excited across the bandgap into the conduction band. This generates electron-hole pairs, with electrons in the conduction band, while the corresponding holes remain in the valence band of the semiconductor. Metal contacts (typically lithographically patterned) apply a voltage bias of around 100 V to 200 V, which serves to accelerate the photo-carriers. Since the semiconductors used for THz-TDS are low-temperature-grown, they exhibit large resistivity ρ and short carrier life-time τ_l[1]. Upon application of the fs-laser and excitation of electrons across the bandgap, ρ decreases since the photo-carriers cause an increase in photoconductivity between the contacts $\left(\rho = \frac{1}{\sigma}\right)$. The resulting transient current emits EM-radiation in the THz range, during the laser pulse. This mechanism can be approximated as dipole radiation, which can be studied using Maxwell's equations.

The magnitude of the transient current produced is a function of the carrier mobility μ of the semiconductor

being excited. It is described by

$$I(t) = Anq(t)\mu E_{\text{inc.}},$$

with A being the cross-sectional area of the conductor, n being the number density of charges, q being the time-dependent charge, and $E_{\text{inc.}}$ being the incident electric field.

The generated THz electric field

$$E_{\text{THz}} \propto \frac{\partial I(t)}{\partial t} \propto \mu$$

implies that increasing μ enhances the rate of change of current, and therefore the amplitude of the emitted E_{THz}, leading to a more efficient generation of E_{THz}.The mobility μ is time-independent, supporting this interpretation. However, it is important to optimise for μ and τ, which are often inversely related, since we want a broad THz spectrum with sufficient amplitude. Different semiconductors have different τ, μ, and other properties, and therefore are also worth comparing, as these might allow for better material characterisation.

After generating a THz signal, it is transmitted through the material under test and then detected in order to characterise the material and obtain $\tilde{n}(\omega)$. As with generation, a number of methods can be used to detect E_{THz}. Commonly, PCA is used to perform coherent sampling. Here, there is no external bias between the lithographically fabricated electrodes. For detection, the E_{THz} field acts as the internal bias and the magnitude of this determines the magnitude of the transient current. The detected photocurrent using this method is weak, making measurements having a high degree of noise, leading to small Dynamic Range (DNR) and Signal-to-Noise Ratio (SNR). In order to address this, a lock-in amplifier is used to average a signal $S(t)$ over some period of time with a time-constant τ, this should not be confused with carrier lifetime. The signal detected is approximately equal to E_{THz} though technically it is proportional to a convolution in the time-domain, $S(t) \propto I_{\text{opt}}(t) * E_{\text{THz}}(t)$; where $I_{\text{opt}}(t)$ is the intensity profile of the laser pulse.

To construct a full profile of the transient THz signal, a delay stage is introduced. This is a mechanical translation stage placed in the path of the laser beam, which varies the relative arrival time between the probe and the THz pulse at the detector. By scanning (the scanning rate) the delay stage and recording the photocurrent at each time step, it is possible to sample the THz waveform in the time domain.

Intuitively, it seems plausible that maximising the time constant τ would maximise SNR since the random noise would destructively interfere by superposition. However, it is also necessary to consider the scanning rate of the delay stage. Ideally 3-5 τ are allowed to elapse per delay step at the sharpest feature of the signal. If the delay stage is moving during this averaging process the signal will be rapidly changing and so a smeared output across time-points of E_{THz} will be recorded. That is, the electric field E_{THz} at a time t is not a good representation of the time-dependent filed, due to large amount of temporal blurring. Furthermore, since sharp peaks are blurred with respect to the weighted average of neighbouring values, high-frequency signals are suppressed reducing the DNR of the system, potentially increasing the uncertainty in $\tilde{n}$ determined.

Finally, to actually obtain $\tilde{n}$, the transfer function of a material of interest is compared relative to a reference. A transfer function is a mathematical expression that describes the output of a system in response to a given input, in this context, it quantifies the response of the sample relative to the reference. Generally, the transfer function takes the following form[1,7]

$$\frac{E_s}{E_{\text{ref}}} = \frac{t_{12}t_{23}}{t_{13}} \cdot \frac{P_2}{P_3} \cdot \frac{\text{FP}_{012}\,\text{FP}_{123}}{\text{FP}_{013}}, \tag{1}$$

where E_s and E_{ref} are the complex electric transfer functions (electric fields) transmitted through the sample and reference respectively, t_{ij} is the transmission Fresnel coefficient, P_i is the propagation factor through layer i and FP_{ijk} is Fabry-Perot Etalon term. Typically the THz-TDS is run in the same configuration with the material mounted and without, with the configuration without the material acting as the reference. The transfer function E is a product of the Fresnel coefficients at the boundaries, given the transfer function can be directly measured and the refractive indices of the known materials are known, along with their thickness, $\tilde{n}$ can then be extracted numerically. Depending on the size of the material relative thicknesses of the sample and substrate (GaAs) a number of further simplifications can be made.

Once $\tilde{n}$ is extracted from use of the analytical expression (or appropriate simplified form) in Eq. 1, secondary parameters can be determined following the definitions detailed in § II. Of particular interest for THz-TDS, the absorption coefficient[8] α is used, as it has significant utility in identifying chemical components in drugs and explosives.

In the derivation of this analytical expression (Eq. 1), detailed by Pupeza, Wilk, and Koch [7], a number of assumptions are made that should be considered when reporting measured material properties such as $\tilde{n}(\omega)$, as they may not hold true for all materials. The investigated sample, that is, the material of interest, is assumed to be homogeneous. The surface is assumed to be smooth, thereby neglecting scattering effects at the interface. A dry atmosphere within the testing equipment is also assumed. This is reasonable, as a dry atmosphere is generally desirable during measurements due to the spurious absorption peaks of water vapour, which introduce unwanted spectral features. These water-related effects mask spectral features of the material of interest [cite]. It is additionally assumed that the THz incident signal is orthogonal to the sample of interest. This introduces some uncertainty when calculating analytical terms from the mea-

sured transfer function, E.

While these assumptions simplify analysis, they also highlight practical limitations of THz-TDS. In reality, not all samples to be characterised are flat, homogeneous, and isotropic. Producing an entirely dry atmosphere might not always be feasible, and if purely transmission mode is adopted it is generally assumed the material is non-magnetic in the derivation. The technique is also sensitive to sample positioning, meaning deviations from the ideal conditions above can lead to measurement errors. These limitations are addressed through comparable techniques in the THz range.

III.B. Magnetic materials ($\mu \neq 1$)

Some samples to be characterised have non-unitary permeability[9], that is, $\mu \neq 1$; in other words, they are magnetic. In this context, to properly characterise a material, both the permittivity and permeability must be considered. THz-TDS can be used for this, although it is a relatively uncommon use case. In order to achieve this using a THz-TDS system, a dual-mode configuration is required[9–11]. This utilises both transmission and reflection measurements to determine both parameters. However, more standard methods for retrieving both $\tilde{\varepsilon}$ and $\tilde{\mu}$ rely on VNAs, particularly in TL configurations.

Shifting from transmission to reflection mode (and vice-versa) can lead to an increase in uncertainty in the results obtained, Ung *et al.*[9] pioneered a method to use a standard THz-TDS system that can measure in both regimes simultaneously. The set-up is largely similar to that of transmission-based THz-TDS described previously. Using four off-axis parabolic mirrors and a Ti:sapphire source with femto-second pulse length, with PCA being used for pulse detection of both transmitted and reflected beams. However, a beam splitter (380 µm thick float-zone silicon wafer) and an additional off-axis parabolic mirror are added.

Using this configuration, both transmission and reflection spectra can be measured:

$$R(\omega) = \frac{E_{\mathrm{s,r}}}{E_{\mathrm{ref,r}}}, \qquad T(\omega) = \frac{E_{\mathrm{s,t}}}{E_{\mathrm{ref,t}}}.$$

These can then, of course, be used to obtain $\tilde{n}$ in either mode from Eq.1 (though of course this requires the assumption that $\tilde{\mu} \approx 1$ which isn't valid in this regime). Ung *et al.*[9] does not discuss how to obtain $\tilde{\mu}$ from this configuration. However, this procedure has been derived and demonstrated previously by Minowa *et al.*[10]. The impedance $\tilde{Z}(\omega)$ can also be calculated directly from $T(\omega)$ and $R(\omega)$. By then utilising the relationship between $\tilde{\varepsilon}$ and $\tilde{\mu}$ in terms of $\tilde{Z}$ and $\tilde{n}$:

$$\tilde{\varepsilon} = \frac{\tilde{n}}{\tilde{Z}}, \qquad \tilde{\mu} = \tilde{n}\tilde{Z},$$

both parameters can be derived, and from these, further secondary parameters of interest can be obtained (§ II).

Whilst an analytical approach can successfully determine both $\tilde{\varepsilon}$ and $\tilde{\mu}$ with reasonable uncertainty[10], a modelling-based approach has also been implemented[11]. In this method, a variational technique minimises the squared error between measured and simulated transmission and reflection spectra. From the resulting fits, $\tilde{n}$ and $\tilde{\mu}$ can be obtained.

Papari *et al.*[11] found that the determined value of $\tilde{\varepsilon}$ for $BiFeO_3$ differed from values reported in the literature when the assumption $\tilde{\mu} \approx 1$ was lifted. Recall that this assumption also enforces $\tilde{\varepsilon} = \tilde{n}^2$, which does not hold if the permeability deviates from unity. By accounting for this, they attributed the discrepancy to a non-unitary permeability, specifically $\mu_r(\omega = 2.3\,\mathrm{THz}) \approx 1.3$. Therefore, a strong argument can be made that applying the initial non-magnetic assumption used by other groups constitutes a fundamental mischaracterisation of the material. Magnetoelectric effects were also observed. This warrants a further investigation of other materials, that might be inappropriately assumed non-magnetic, under characterisation.

However, as briefly stated, this method is less frequently utilised than VNA-based approaches for the characterisation of magnetic materials, such as magnetic dielectrics or metamaterials.

III.C. Relevant Applications

A number of studies from the early 2000s proposed the use of THz-TDS for the identification of narcotics and explosives; with possible security scanner and defence applications. Notably, Davies *et al.*[8], reviewed how illicit substances could be distinguished by plotting the evolution of the absorption coefficient α as a function of frequency ω, and identifying characteristic spectroscopic fingerprints relative to a cardboard reference. This approach is particularly relevant in the context of scanning packages.

Figure 1 shows a plot of α against ω for various substances, highlighting how different chemical compositions feature differing absorption spectra. By comparing these with measured spectra, identification of these chemicals is possible through packages by subtracting the absorption of the cardboard[8].

More recently, some work has been focused on improving the analysis of obtained spectra. Traditionally, Principal Component Analysis[12] is used for pre-processing of spectra. This technique, however, struggles with more complex samples. Wang *et al.*[12] used a Convolution Neural Network (CNN) that proved significantly more successful than traditional techniques, identifying 100% of the high SNR samples and 98.6% of the low SNR samples, compared to $\sim$ 85% with existing techniques. Li *et al.*[13] used Voigt (a probability distribution from

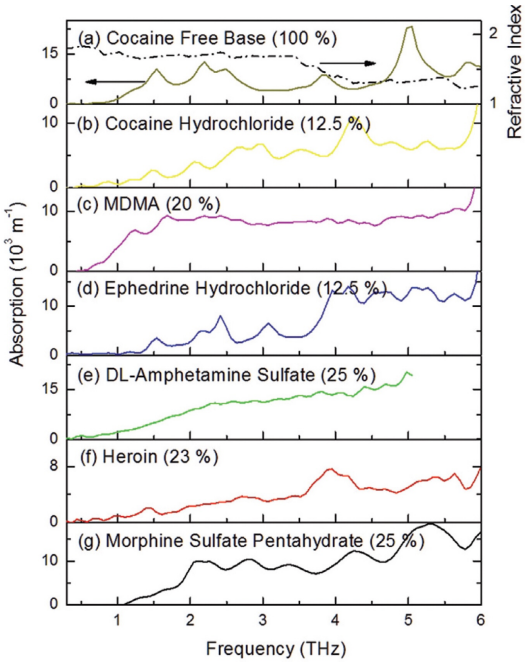

Figure 1 | Absorption spectra against Frequency for a number of illicit substances. Figure demonstrates unique spectroscopic fingerprints for the substances plotted. Figure taken from Davies *et al.* [8].

convolving a Lorentzian and Gaussian) and Asymmetric Least Squares (AsLS) to reconstruct absorption peaks for substances found in simulated mail. Issues arise from the air gaps in the packaging, and the use of fitting here aims to help address this. AsLS was used for baseline correction, and then Voigt fitting was used to reconstruct the peaks. This method proved effective at reducing the impact of the air gaps, leading to an improvement of approximately $\sim 10\%$. Importantly, this work uses pre-existing measurement procedures and equipment commonly adopted for THz-TDS, reducing redundancy but enhancing measurement outcomes. However, there are currently a number of limitations identified for this procedure that are worthy of further investigation; smaller absorption peaks are often lost when fitting the spectral data due to being mischaracterised as noise. This is an issue, since these peaks could be essential in the identification of some chemical compounds. Furthermore, some complex compounds have overlapping absorption peaks that are problematic when fitting. Further refinement of the algorithms used for this spectral fitting aims to address these shortcomings.

IV. ELLIPSOMETRY (REFERENCE-FREE THZ-TDS)

Ellipsometry[14] is a well-defined technique used to extract amplitude and phase information of a wave after being reflected from a material, thus characterising the optical properties or refractive index $\tilde{n}$ of some material.

Traditional (transmission-based) THz-TDS requires *a priori* information about the object under test. Furthermore, Friederich *et al.* [14] report the challenges of using transmission-based THz-TDS for highly absorbing liquid samples and suggest the use of reflection-based THz-TDS as a solution. However, this method requires a reference to compare the measurements to—the *a priori* information. This is not always possible.

Combining ellipsometry with a THz-TDS set-up is presented as a way to improve reflection-based THz-TDS and aims to eliminate the need for this *a priori* knowledge. This has the advantage of not only characterising material parameters but also demonstrates an ability to study the object's shape and positioning. Often, with THz-TDS, sample positioning is highly important and can contribute to the uncertainty in the measurement, whereas in this technique, the sample positioning and object shape are determined experimentally[1,14].

The THz-TDS is used under a standard configuration[1], in agreement with those discussed previously. It features a femtosecond laser source and an LT-GaAs substrate. In adopting this method, no mirrors or lenses are needed to collimate the beams. This is in direct contrast to other FS approaches, such as a FS-VNA or standard THz-TDS[1,15,16]. This does, however, necessitate calibration—something which traditional THz-TDS does not.

This ellipsometric method works by comparing s- and p-polarised light and their respective reflection coefficients, R_s and R_p. These are expressed as a ratio[17]:

$$\frac{R_p}{R_s} = \tan(\Psi) \cdot e^{i\Delta},$$

where Δ is the phase shift between the components, and Ψ is the amplitude ratio between the polarisation states.

To determine these parameters, the ellipsometer sets the polarisation state of the incident beam (typically at a fixed angle such as $\theta_i = 45°$). The change in the polarisation state of the reflected beam is then measured, and the ellipsometric parameters Ψ and Δ are determined directly from the ratio of the reflected p- and s-components.

To prevent the impact of dispersive effects of the material being characterised, Kirchhoff imaging is adopted to identify contours and flat parts of the objects. Material parameters are calculated exclusively by the flat edges (specular reflection); this is done using Fresnel coefficients for s- and p-polarised light. Again, this is largely in line with standard post-processing of THz-TDS data[1].

This novel technique demonstrates the ability to calculate refractive indices to a reasonable degree of accuracy, $n_{\text{measured}} = 3.02$ vs. $n_{\text{known}} \approx 3.10$, even for small objects with relatively complex geometries. This technique is also only capable of determining $\tilde{\varepsilon}$, since it avoids the use of transmission-based THz-TDS; to extract both $\tilde{\varepsilon}$ and $\tilde{\mu}$, measurements in both transmission and reflection modes are required. Therefore, its applicability is limited to non-magnetic materials and it cannot be used to

characterise magnetic or metamaterial samples.

Finally, this method is preferred over VNA-based techniques for certain non-magnetic materials with unknown geometry, poor alignability, and high absorption.

V. BROAD OVERVIEW OF TRANSMISSION LINE VNA

The following section is broadly based on work performed by Naftaly et al. [2].

VNA measurements are the primary TL method used for device and material characterisation[2]. Waveguides are typically employed to direct the EM-wave through the material. These waveguides are used to obtain measurements with a VNA. The frequency of the THz wave is often lower relative to THz-TDS, with frequencies around 0.2 THz, the lower end of the THz band. They are commonly used in the GHz range for characterising RF-devices. A typical schematic for a VNA in TL configuration is shown in Figure 2.

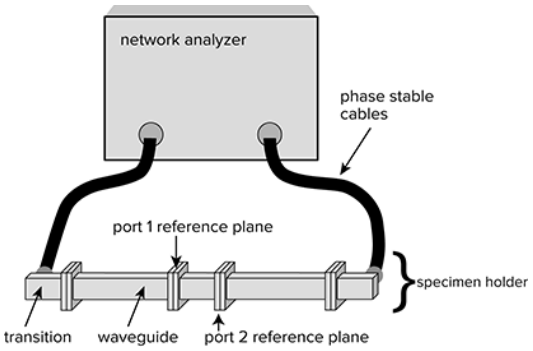

Figure 2 | Schematic showing the set-up required to extract $\tilde{\varepsilon}$ from a VNA in a TL configuration. A waveguide ser the transmission medium. Taken from the ATSM-D5568-22a[18].

A VNA is used to determine S-parameters (scattering parameters). These take the form S_{ij}, where i and j refer to the ports the wave enters and exits, respectively. For example, S_{11} represents the reflection at port 1, corresponding to a wave that is incident on and reflected from the same port. As with THz-TDS, the results are complex in nature, so both phase and magnitude information are reported. Often[4], it is assumed that S_{11} and S_{22} are equal. This is valid under the assumptions of an isotropic and homogeneous sample. The interfaces (waveguides) are also assumed to be identical. In addition, S_{21} and S_{12} are assumed equal if there is no directional bias and the system is reciprocal.

Prior to taking a measurement with a VNA, the equipment is calibrated to reduce systematic errors. This is in contrast to THz-TDS but akin to ellipsometry. This is done by Through-Reflect-Line (TRL). Briefly, three measurements are taken: a direct connection between the two ports (Through), a known high-reflectance (Reflect), and a transmission line of known length (Line). These measurements are used to solve for the systematic error terms at each port of a VNA. Several considerations[18] should be made after calibration to ensure ideal data acquisition: the same cable used for calibration should be used, S-parameter results should be tested on a known specimen, and calibration lasts for an hour before the need for re-verification.

This allows determined S-parameters to be representative of the material or device being tested and not intrinsically linked to the particular VNA being used.

When taking measurements with a VNA, care must be taken to avoid voids. That is, the material or device being characterised must fill the sample holder. This is because voids would affect the measured transmission coefficient S_{21}.

Once S-parameters are determined, a number of data-reduction inversion algorithms exist to convert from these parameters to the complex relative permittivity[18,19]

$$S_{ij} \to \tilde{\varepsilon}_r \stackrel{\text{def}}{=} \frac{|\boldsymbol{D}|}{\varepsilon_0 |\boldsymbol{E}|}.$$

Before employing an algorithm, a phase correction is made to the transmission S-parameters (S_{21}, S_{12}) to account for the TL length displaced by the sample — that is, to account for the length of the sample. From here, an algorithm is used. The choice of algorithm depends on either sample positioning or some initial guess. Naftaly *et al.* [2] used the *iterative one-parameter* method detailed by the ATSM[18]. Essentially, $\tilde{\varepsilon}$ is initially guessed and through a series of equations S_{21} is calculated and compared to the measured value. The guess is then adjusted until the S_{21} value determined by $\tilde{\varepsilon}$ matches the one that was measured.

However, other methods are popular for the determination of $\tilde{\varepsilon}$ from S-parameters. These are summarised in Tab. I.

Table I Table summarising the four main inversion algorithms to determine $\tilde{\varepsilon}$ from one or more S-parameters. ATSM[18].

Algorithm	S-parameters used	Requirement	Solves for $\tilde{\mu}_r$
NRW	S_{11}, S_{21}	Sample position	Yes
Iterative four-parameter	$S_{11}, S_{22}, S_{21}, S_{12}$	Initial guess	Yes
Modified NRW	S_{11}, S_{21}	Sample position	No
Iterative one-parameter	S_{21}	Initial guess	No

The choice of algorithm is motivated based on the sample properties[18], with different algorithms have distinct merits. The Nicholson, Ross and Weir (NRW) algorithm is used for magnetic samples ($\tilde{\mu} \neq 1$), however it has known

numeric instability when

$$\omega = \frac{n\lambda}{2}, \quad n \in \mathbb{Z}_+.$$

Modified NRW is suitable for non-magnetic samples ($\tilde{\mu} \approx 1$), this modified algorithm no longer as the numerical instability. Iterative four-parameter is suitable for magnetic (and non-magnetic) materials where the location within the set-up is not known to a high degree of accuracy. The initial guess can be verified based on the stability of both $\tilde{\varepsilon}$ and $\tilde{\mu}_r$. Finally, iterative one-parameter is for a non-magnetic material with some known permittivity. This approach is largely similar to that of the iterative four-parameter approach, but is computationally simpler.

Modifications to the (hollow) Waveguide Rectangular (WR) can be made[20], with different WRs supporting different frequency bands (these are often referred to as WM – an equivalent metric standard). This allows the extension of the VNA to greater frequencies, allowing for a greater spatial resolution ($\lambda \propto 1/\nu$). Each WR operates above a specific cut-off frequency, determined by its geometry, to ensure single-mode propagation. Following guidelines from IEEE[20], WR selection is an important parameter of consideration when using a TL VNA; it is known to affect recorded electrical properties (transmission loss and return losses). For each waveguide in the standard[21], the reflection coefficients R are reported by IEEE across the frequency band, as well as uncertainty estimations.

In the above a VNA has been discussed using a waveguide, that is, as a TL-method. However, a VNA can also be used in a free-space configuration. This expands the capabilities of a VNA

V.A. Use of Material Characterisation Kits (MCKs) (guided FS method)

"Material Characterisation Kits (MCKs)[15] are used for measurement of the permittivity" and are often discussed in the context of the loss angle of planar specimens at room temperature. They use a standard VNA, a traditionally a TL-method, in a quasi-FS regime. As described previously, $\tilde{\varepsilon}$ is determined through an inversion algorithm and iterative fitting of S-parameters. A schematic of an MCK is shown in Figure 3.

MCKs feature two corrugated horn antennas which act to focus the THz beam[3]. The beam is then focussed by a series of mirrors and/or lenses, with the sample being place at the beam (horn) waist, as demonstrated in Figure 3. This allows a VNA to work in a quasi-free-space configuration. However, this set-up generally has issues with respect to multiple reflections, that can cause issues with measurement-based artefacts if not appropriately accounted for. These are known to be difficult to remove with calibration, typically this is addressed by various filtering techniques (Savitzky-Golay filter and time-gating)[3,22].

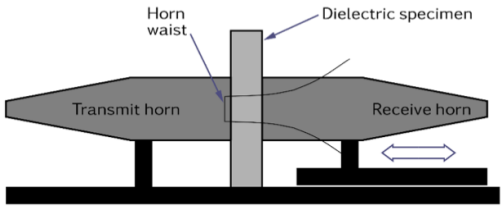

Figure 3 | A schematic of an MCK, used to determine $\tilde{\varepsilon}$ when paired with a VNA. The transmit horn converts the guided wave into a quasi-plane wave that passes through the material being characterised. The receive horn then collects the transmitted wave and converts it back into a guided wave to obtain the S-parameters. Figure taken from Naftaly [15].

However[23], FS-based methods do have a few drawbacks compared to TL-based characterisation: there are instances where the algorithms used to analyse data are based on another simplification of the beams used, e.g., assuming the incident waves are perfect plane waves. Whilst the use of a MCK attempts to ensure this, it is still nonetheless an assumption. Moreover, the sample position could be incorrect, disagreeing with the theory.

VI. FTIR IN THZ RANGE

This technique has been used in the THz range[4]. It is based on the Fourier transform of a recorded interferogram from a Michelson interferometer. It has the primary advantage of covering an extremely wide frequency band (0.1 THz to 10 THz). To obtain n and κ, interference fringes are counted, and the sample dimensions are taken into account. The refractive index is given by:

$$n(\nu) = \frac{mc}{2L\cos\delta \cdot \nu(m)},$$

where m is the interference order, L is the sample thickness, and δ is the internal tilt angle. The extinction coefficient is given by:

$$\kappa(\nu) = -\frac{c\ln(T)}{4\pi\nu L\cos\delta}.$$

Since, FTIR relies on the identification of fringe (peaks and troughs), therefore for highly absorption samples it becomes challenging to determine n and κ. δ, L and Δm are all known to contribute to the uncertainty in the determination of n and κ.

VII. COMPARISONS

Recent publications[3,4,16] demonstrated that THz-TDS, TL VNA, FS VNA, and FTIR can achieve comparable accuracy in determining $\tilde{\varepsilon}$. However, some discrepancies arise under more challenging conditions. For in-

stance, Shang *et al.*[3] observed that when characterising materials with higher $\tilde{\varepsilon}$, variation between measurements using THz-TDS and VNA with a MCK increased, with THz-TDS occasionally producing non-physical values of the loss angle (§ II). This issue was not observed in VNA with MCK measurements, although they were generally noisier than those from THz-TDS and other techniques. Indeed, Oberto *et al.*[4] found that THz-TDS in some instances reported negative values for the extinction coefficient κ, which is unphysical for passive materials. This occurred in the low-κ materials (quartz and pyrex). Most of this uncertainty appears to arise from Fabry–Pérot reflections and sample thickness. Moreover, for highly absorbing materials (BK7), FTIR struggled to reliably characterise the material. Further agreement in terms of uncertainty was reported, with THz-TDS generally having the smallest uncertainty across the materials tested. The following analysis discusses frequency bands, geometric constraints, calibration needs, and the property-measurement capabilities of each method. Tab. II presents a side-by-side summary of these findings.

Kato and Kato[16] introduced a novel approach using Frequency Selective Surfacess (FSSs) to create materials with artificially controlled dispersion $\left(\frac{\mathrm{d}[\mathrm{Re}(\tilde{n})]}{\mathrm{d}\omega} \neq 0\right)$. Often, materials characterised in the mm-frequency range lack significant variation of $\tilde{\varepsilon}$ with frequency ω; this means such systems might not be well-suited to capture sharp changes in material properties with frequency. Results were benchmarked against simulations over the D-band (>0.11 THz) and J-band (>0.22 THz) frequency ranges. Both systems (THz-TDS and FS-VNA) showed good agreement with simulated data, though minor deviations were attributed to oblique incidence and fabrication inconsistencies. This supports the view that THz-TDS and VNA-based methods offer similar capabilities for free-space characterisation, even in complex scenarios. Performing similar work at higher frequencies in the THz band is the next logical step to ensure that this conclusion holds across a wider, experimentally relevant frequency range.

Across all studies, it is important to note that the frequency band of FTIR is the broadest (0.2 THz to 6 THz), followed by THz-TDS (0.25 THz to 2.5 THz), and then the VNA (0.3 THz to 0.5 THz). Therefore, all measurements reported in these studies were conducted at relatively low frequencies within the THz band (< 0.5 THz). This prompts further questions about the limitations of equipment in a higher ω limit. It is known that, at least for THz-TDS, using higher frequencies increases the sensitivity of the equipment[24]. The comparisons discussed here do not exhibit this behaviour for THz-TDS. A comparison at higher frequencies would allow this behaviour to be evaluated, since capable VNAs do now exist. Nevertheless, under current sensitivity constraints, broad agreement between both systems and simulations was achieved across all papers.

In these studies, equipment was deployed in standard configurations consistent with the wider literature[1,15]. For THz-TDS, PCA was used for both emission and detection, with E_{THz} measured optically[16] or via a delay line[3]. The VNA system resembled a quasi-free-space setup using a MCK; however, in the case of Kato and Kato[16], transmission and receiving horns were not adopted, preventing plane-wave-like illumination.

It would be interesting to see if introducing MCKs to the setup in Kato and Kato[16] would reduce oblique incidence errors, as the corrugated horns assist in producing plane-wave-like incident light at the VNA. Despite measurements between THz-TDS and VNA being largely similar, this could provide further merit for the VNA, as a major contributor to error could be mitigated. This could bridge the gap in reported uncertainty between VNA and THz-TDS.

Other differences exist in terms of measurement requirements. To obtain measurements using a VNA in a FS or TL configuration, the system must be calibrated using a TRL approach. However, producing consistent TRL results is challenging at mm-wavelengths[25]. THz-TDS does not have this issue, as it takes measurements relative to a reference spectrum, typically from an empty sample or substrate[1]. When using THz-TDS, many systematic errors cancel out when reporting the ratio of E_s/E_{ref}. This means calibration-dependent errors can be bypassed in THz-TDS, relative to a VNA-based system. In addition, for some plastic materials refractive index measurements from THz-TDS are known to vary due to hygroscopicity[26]. Furthermore, what is not often made explicit in discussions of ellipsometry[14,27] is why it may be advantageous compared to a FS-VNA, which, like ellipsometry (and unlike traditional THz-TDS), does not require any *a priori* information. Its main advantage appears to be a reduced sensitivity to precise sample positioning.

Across all papers compared here, the complex dielectric constant $\tilde{\varepsilon}$ was predominantly discussed, while the determination of permeability $\tilde{\mu}$ was less frequently considered a material parameter of interest. A common assumption is that materials are non-magnetic and exhibit negligible magnetic response at THz frequencies ($\tilde{\mu} \approx 1$), which justifies the simplification $\tilde{\varepsilon} = \tilde{n}^2$.

For magnetic materials, the choice of technique is limited relative to that of non-magnetic ones. In the above, we have discussed how THz-TDS can be used in a dual-mode configuration of both transmission and reflection to determine $\tilde{\varepsilon}$ and $\tilde{\mu}$, and how the same is true if all four S-parameters are used. Ellipsometry and FTIR are incapable of this determination. It is also worth noting that, in both of these configurations (THz-TDS and VNA), calculations involving $\tilde{\mu}$ are considerably more sparse than those exploring $\tilde{\varepsilon}$, and some future testing directly com-

paring the determined $\tilde{\mu}$ from VNA in TL and FS, and from THz-TDS, should be performed in much the same way as previous works have done for $\tilde{\varepsilon}$.

Furthermore, the ability to determine secondary parameters, as discussed in §II, is clearly limited for techniques that do not explicitly measure both phase and magnitude (FTIR). This reduces their usefulness when the material is being studied in terms of losses (dielectric or magnetic), impedance, or absorption. That is, beyond broadly characterising the real components or applying numerical methods, these techniques face fundamental limitations.

In addition to the instrumental and algorithmic factors discussed, practical constraints related to sample geometry and type must also be considered. These limitations can restrict the choice of technique before other factors even come into play, as certain materials may be practically incompatible with specific measurement methods. Notably[2], a TL-VNA configuration requires that the sample completely fills the waveguide cross-section, with no voids present. Hence, powdered samples are often desirable. For ellipsometry[14], samples need to be weakly absorbing and relatively thin. If the samples are sufficiently thick—on the order of the wavelength of the incident beam (10 µm to 300 µm)—there is an increased risk of multiple reflections, and therefore, measurement error[27]. This is due to overlapping internal reflections that distort the phase and amplitude of the reflected beam. FTIR[4] struggles with highly absorbing materials, since it relies on detectable interference fringes, which may not form clearly in such cases. FS THz-TDS and VNA-based methods require flat samples of moderate thickness. Withayachumnankul, Fischer, and Abbott[28] demonstrated that the optimal thickness l_{opt} is frequency dependent and can be calculated from the absorption coefficient as

$$l_{\text{opt}} = \frac{2}{\alpha(\omega)} = \frac{c}{\omega\kappa(\omega)}.$$

If the material is too thin, it is difficult to transmit a THz signal that differs significantly from the reference spectrum through the sample[28]. If it is too thick, the bulk can indeed be more effectively characterised; however, the SNR is reduced due to increased attenuation. In practice, an optimal thickness of approximately 1 mm is suitable for highly absorbing samples, while for weakly absorbing materials, a thickness closer to 100 mm is more appropriate. This makes the measurement of thin films or objects with a small radius of curvature difficult to perform accurately.

Generally, the key takeaway from these papers is that the choice of method should depend on both the geometric and intrinsic properties of the material being tested, as well as the desired spectral range. This highlights the importance of selecting an optimal technique to improve the quality of data acquisition.

VIII. CONCLUSIONS AND SOME THOUGHTS ON THE FUTURE DIRECTION

Throughout this review, the merits and limitations of the key techniques used for THz-based material characterisation have been discussed and compared. However, several real-world challenges remain that limit the broader adoption and future development of these methods. To enable wider implementation[23], measurement times must be reduced. In addition, lowering the cost and reducing the physical footprint of THz systems would further support their integration into industrial settings. Often, the spatial resolution of the techniques discussed here are too low to characterise emerging materials with orders of magnitude (e.g. nanoparticles) smaller than can be achieved with THz-TDS. Moreover, for materials with weak absorption of THz-radiation, many techniques fail to get sufficient SNR.

This review supports the utility and investment in THz-based material characterisation and aims to improve the reader's understanding of the specific advantages of different techniques, given information about the sample under test.

In terms of an over-arching technique, THz-TDS largely performs the most consistently, featuring a relatively wide frequency band and low general uncertainty. It is capable of determining both $\tilde{\varepsilon}$ and $\tilde{\mu}$, and modifying it to be in an ellipsometric configuration reduces the constraints on sample positioning. Therefore, if a single piece of equipment had to be adopted by a lab, the recommendation is THz-TDS.

Table II Comparison of THz-TDS and VNA-based characterisation methods .

	THz-TDS		VNA		
Metric	**FS**	**Ellipsometry**	**TL**	**FS / MCK**	**FTIR**
Frequency Range	∼1 THz	> 6.5 THz	0.140 THz to 0.220 THz	0.110 THz to 0.330 THz	0.1 THz to 10 THz
Fundamental Material Properties	$\tilde{\varepsilon}$ and $\tilde{\mu}$ (if both transmission and reflection modes), else $\tilde{\varepsilon}$	$\tilde{\varepsilon}$	$\tilde{\varepsilon}$ and $\tilde{\mu}$ (if using four S-parameters), else $\tilde{\varepsilon}$	$\tilde{\varepsilon}$ and $\tilde{\mu}$ (if using four S-parameters), else $\tilde{\varepsilon}$	$\tilde{\varepsilon}$ (using interferometer or Kramers-Kronig)
Sample Type	Flat and isotropic. $l_{\text{opt}} \approx$ 1 mm to 100 mm depending on α	High absorption materials, thickness < 50 µm	Solid dielectrics. Completely fill waveguide (voidless)	Anisotropic samples, FSSs. $l_{\text{opt}} \approx$ 1 mm to 100 mm depending on α	Weakly absorbing, flat samples with measurable fringes
General Ranked Accuracy	1	4	2	3	5
Measurement output	E_{THz} (Magnitude and Phase)	E_{THz}, s- and p-polarisation (Magnitude and Phase)	S-parameters (Magnitude and Phase)	S-parameters (Magnitude and Phase)	$T(\nu) = \frac{I_{\text{sample}}(\nu)}{I_{\text{ref}}(\nu)}$ (Magnitude)
Calibration	None, reference measurement	Reference-free, needs calibration for precise measurement of material parameters	TRL	TRL	None
Main Limitations	Requires dry atmosphere, homogeneous and smooth samples, and $E_{\text{THz}} \perp$ surface. Non-physical artefacts may arise for sharp variations in $\tilde{\varepsilon}(\omega)$. Retrieval is challenging when $\lambda_{\text{THz}} \approx$ sample size or when thickness exceeds skin depth δ.	Air-gaps lead to poor measurements. Position or an initial guess is needed to determine $\tilde{\varepsilon}$. Variations in specimen holder dimensions, uncertainty in specimen length. Line losses and connector mismatch.	Susceptible to problematic multi-reflections and calibration drift. Assumes incident wavefronts are planar	Fails for highly absorbing samples; accuracy depends on geometry	No explicit phase measurement; secondary parameters require analytical retrieval
Key Applications	Detection of drugs and explosives. Highly popular method for general material characterisation generally.	Non-planar samples, poor alignment	RF evaluation at mm-wave	Metamaterials	Thin polymer coatings
Future Direction	Use of CNNs and developments in spectral fitting	3D sample characterisation and shape-based extraction	–	Handling oblique incidence	General improvement for absorbing materials, perhaps by implementing ATR.
Key References	2,3,8,12,13,15	14	15,16,18	2,4,18	4

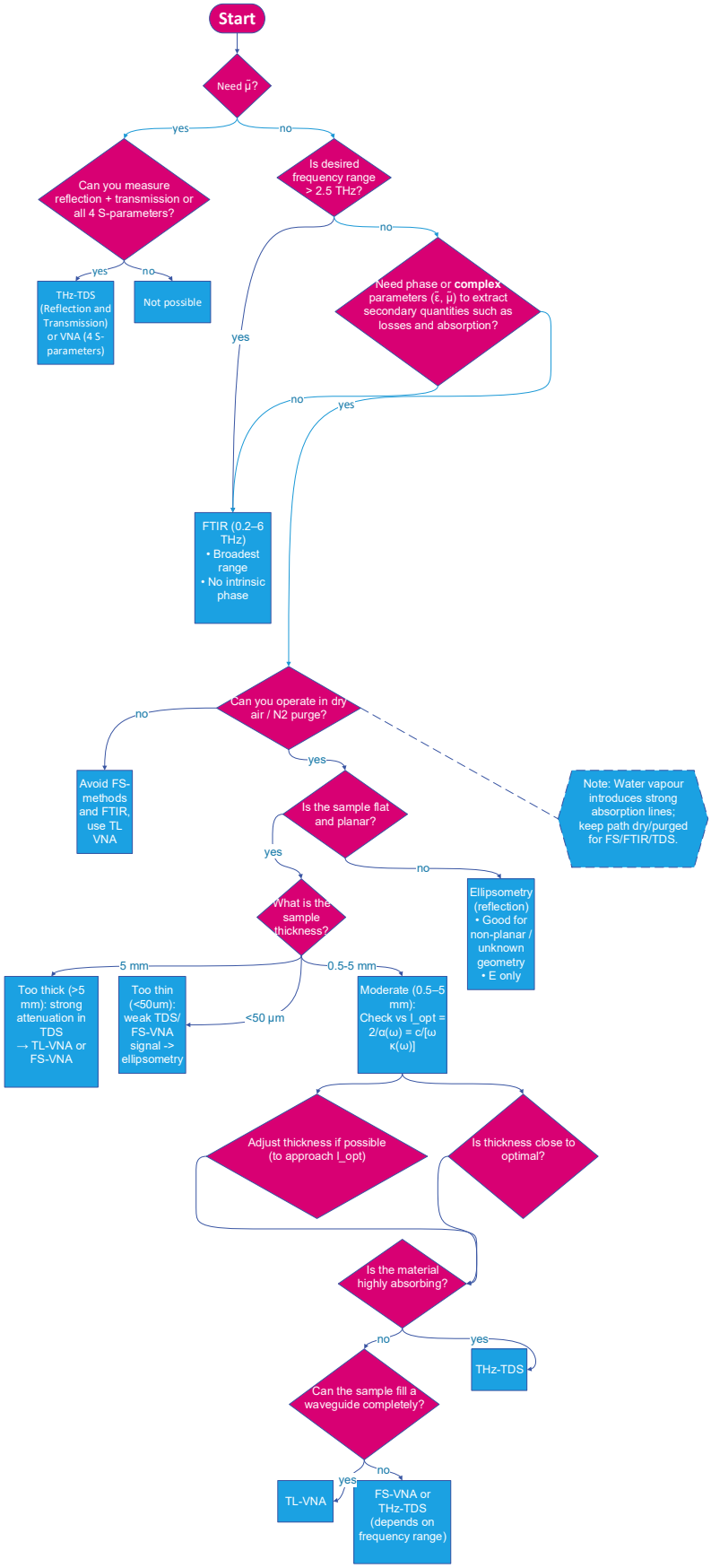

Figure 4 | Flowchart illustrating the decision-making process for selecting THz characterisation techniques, derived from the literature review, based on sample type and geometry. Decisions are largely based on information summarised in Tab. II.

ACKNOWLEDGMENTS

The author gratefully acknowledges the School of Physics and Astronomy at the University of Edinburgh for awarding a Career Development Summer Scholarship, which made this project possible. The work was carried out in formal collaboration with QinetiQ.

Appendix A: Qualitative discussions

As part of this work, I organised meetings with Dr. Mario Gonzalez Jimenez (University of Glasgow, Chemical Photonics) and Tomas Pires (University of Glasgow, PhD student in THz metasurfaces). This appendix outlines the key takeaways from these meetings and from my visit to the University of Glasgow. During our discussions, we focused on the real-world applications of THz measurement methods in both chemistry and metasurface characterisation.

Several useful insights became apparent from these conversations. Primarily, at least in chemical photonics, the measurement of phase is largely irrelevant, and therefore priority was given to methods that are easy to use and highly consistent, with a large SNR and DNR. As a result, FTIR is commonly adopted, even though multiple THz-TDS set-ups are available. This is due to its large frequency band and ease of use relative to THz-TDS. Practically speaking, the THz-TDS set-up has a considerably larger spatial footprint and requires meticulous mirror alignment and laser configuration. Parameter extraction is much simpler for FTIR, and the advantages of intrinsic phase acquisition in THz-TDS are not relevant in all contexts.

However, for metasurfaces, THz-TDS is often preferred, as extracting the full complex refractive index $\tilde{n}$ is typically required to fully describe resonant frequencies and dispersion phenomena. Indeed, Tomas acknowledged that FS-VNA could likely perform the same tasks; however, it is often the equipment that is available and familiar that guides what device is tested, not minimal specific differences.

In both cases, non-magnetic materials were assumed, prompting a comparison between VNA and THz-TDS.The THz-TDS set-up in the chemical photonics lab has previously been configured in reflection mode, suggesting this would be entirely within the scope of the equipment.

More interestingly, one of the key takeaways was the declining interest in THz methods over the past decade. Dr. Mario Gonzalez Jimenez initially worked extensively with THz-TDS 13 years ago, but has since transitioned to using only FTIR, primarily due to its ease of use. That is, for an end user who simply needs to extract material properties, incremental improvements in technology appear to offer minimal practical benefit.

REFERENCES

[1] J. Neu and C. A. Schmuttenmaer, "Tutorial: An introduction to terahertz time domain spectroscopy (THz-TDS)," Journal of Applied Physics **124** (2018), 10.1063/1.5047659, publisher: AIP Publishing.

[2] M. Naftaly, N. Shoaib, D. Stokes, and N. M. Ridler, "Intercomparison of Terahertz Dielectric Measurements Using Vector Network Analyzer and Time-Domain Spectrometer," Journal of Infrared, Millimeter, and Terahertz Waves **37**, 691–702 (2016), publisher: Springer Science and Business Media LLC.

[3] X. Shang, M. Naftaly, J. Skinner, L. Ausden, A. Gregory, N. M. Ridler, U. Arz, G. Ngoc Phung, D. Ulm, T. Kleine-Ostmann, D. Allal, M. Wojciechowski, A. Kazemipour, G. Gäumann, and M. Hudlička, "Interlaboratory Comparison of Dielectric Measurements From Microwave to Terahertz Frequencies Using VNA-Based and Optical-Based Methods," IEEE Transactions on Microwave Theory and Techniques **72**, 6473–6484 (2024), publisher: Institute of Electrical and Electronics Engineers (IEEE).

[4] L. Oberto, M. Bisi, A. Kazemipour, A. Steiger, T. Kleine-Ostmann, and T. Schrader, "Measurement comparison among time-domain, FTIR and VNA-based spectrometers in the THz frequency range," Metrologia **54**, 77–84 (2017), publisher: IOP Publishing.

[5] L.-F. Shi, A. Zahid, A. Ren, M. Z. Ali, H. Yue, M. A. Imran, Y. Shi, and Q. H. Abbasi, "The perspectives and trends of THz technology in material research for future communication - a comprehensive review," Physica Scripta **98**, 065006 (2023), publisher: IOP Publishing.

[6] N. A. Ukirade, "A review on advancement of materials for terahertz applications," Next Materials **6**, 100479 (2025), publisher: Elsevier BV.

[7] I. Pupeza, R. Wilk, and M. Koch, "Highly accurate optical material parameter determination with THz time-domain spectroscopy," Optics Express **15**, 4335 (2007), publisher: Optica Publishing Group.

[8] A. G. Davies, A. D. Burnett, W. Fan, E. H. Linfield, and J. E. Cunningham, "Terahertz spectroscopy of explosives and drugs," Materials Today **11**, 18–26 (2008), publisher: Elsevier BV.

[9] B. S.-Y. Ung, J. Li, H. Lin, B. M. Fischer, W. Withayachumnankul, and D. Abbott, "Dual-Mode Terahertz Time-Domain Spectroscopy System," IEEE Transactions on Terahertz Science and Technology **3**, 216–220 (2013).

[10] Y. Minowa, T. Fujii, M. Nagai, T. Ochiai, K. Sakoda, K. Hirao, and K. Tanaka, "Evaluation of effective electric permittivity and magnetic permeability in metamaterial slabs by terahertz time-domain spectroscopy," Optics Express **16**, 4785 (2008).

[11] G. P. Papari, Z. Mazaheri, F. Lo Presti, G. Malandrino, and A. Andreone, "Accurate THz measurements of permittivity and permeability of BiFeO3 thin films," Optics Communications **586**, 131872 (2025).

[12] C. Wang, F. Shi, M. Zhao, J. Ao, C. Jia, and S. Chen, "Convolutional Neural Network-Based Terahertz Spectral Classification of Liquid Contraband for Security Inspection," IEEE Sensors Journal **21**, 18955–18963 (2021), publisher: Institute of Electrical and Electronics Engineers (IEEE).

[13] T. Li, Y. Gu, C. Wang, Y. Yao, Y. Zhang, Y. Guo, and D. Gu, "Identification of Hazardous Substances in Mail by Terahertz Radiation Based on Voigt and AsLS Fitting Spectral Reconstruction," International Journal of Optics **2025** (2025), 10.1155/ijo/5636677, publisher: Wiley.

[14] B. Friederich, D. Damyanov, J. C. Balzer, and T. Schultze, "Reference-Free Material Characterisation of Objects Based on Terahertz Ellipsometry," IEEE Access **8**, 186138–186147 (2020), publisher: Institute of Electrical and Electronics Engineers (IEEE).

[15] M. Naftaly, "Material Characterisation Kits for measurement of complex permittivity in the frequency range 50 GHz to 750 GHz," (2021).

[16] Y. Kato and E. Kato, "Comparison of free-space VNA and TDS measurements using transmission-type frequency selective surfaces," Microwave and Optical Technology Letters **65**, 2201–2209 (2023), publisher: Wiley.

[17]E. Hecht, *Optics*, 5th ed. (Pearson, Boston Columbus Indianapolis New York San Francisco Amsterdam Cape Town Dubai London Madrid Milan Munich, 2017).
[18]D09 Committee, "Test Method for Measuring Relative Complex Permittivity and Relative Magnetic Permeability of Solid Materials at Microwave Frequencies Using Waveguide," .
[19]D. J. Griffiths, *Introduction to Electrodynamics*, 5th ed. (Cambridge University Press, 2023).
[20]N. M. Ridler and R. A. Ginleyt, "A review of the IEEE 1785 standards for rectangular waveguides above 110 GHz," in *2017 89th ARFTG Microwave Measurement Conference (ARFTG)* (IEEE, Honololu, HI, USA, 2017) pp. 1–4.
[21]"IEEE Recommended Practice for Rectangular Metallic Waveguides and Their Interfaces for Frequencies of 110 GHz and Above–Part 3: Recommendations for Performance and Uncertainty Specifications," ISBN: 9781504421966.
[22]D. Ma, X. Shang, N. M. Ridler, and W. Wu, "Assessing the Impact of Data Filtering Techniques on Material Characterization at Millimeter-Wave Frequencies," IEEE Transactions on Instrumentation and Measurement **70**, 1–4 (2021), publisher: Institute of Electrical and Electronics Engineers (IEEE).
[23]A. Leitenstorfer, A. S. Moskalenko, T. Kampfrath, J. Kono, E. Castro-Camus, K. Peng, N. Qureshi, D. Turchinovich, K. Tanaka, A. G. Markelz, M. Havenith, C. Hough, H. J. Joyce, W. J. Padilla, B. Zhou, K.-Y. Kim, X.-C. Zhang, P. U. Jepsen, S. Dhillon, M. Vitiello, E. Linfield, A. G. Davies, M. C. Hoffmann, R. Lewis, M. Tonouchi, P. Klarskov, T. S. Seifert, Y. A. Gerasimenko, D. Mihailovic, R. Huber, J. L. Boland, O. Mitrofanov, P. Dean, B. N. Ellison, P. G. Huggard, S. P. Rea, C. Walker, D. T. Leisawitz, J. R. Gao, C. Li, Q. Chen, G. Valušis, V. P. Wallace, E. Pickwell-MacPherson, X. Shang, J. Hesler, N. Ridler, C. C. Renaud, I. Kallfass, T. Nagatsuma, J. A. Zeitler, D. Arnone, M. B. Johnston, and J. Cunningham, "The 2023 terahertz science and technology roadmap," Journal of Physics D: Applied Physics **56**, 223001 (2023).
[24]M. Fan, B. Cao, and G. Tian, "Enhanced Measurement of Paper Basis Weight Using Phase Shift in Terahertz Time-Domain Spectroscopy," Journal of Sensors **2017**, 1–14 (2017), publisher: Wiley.
[25]"Simplifying the Art of Terahertz Measurements," (2023).
[26]W. Withayachumnankul, G. M. Png, X. Yin, S. Atakaramians, I. Jones, H. Lin, B. S. Y. Ung, J. Balakrishnan, B. W.-H. Ng, B. Ferguson, S. P. Mickan, B. M. Fischer, and D. Abbott, "T-Ray Sensing and Imaging," Proceedings of the IEEE **95**, 1528–1558 (2007).
[27]X. Chen and E. Pickwell-MacPherson, "An introduction to terahertz time-domain spectroscopic ellipsometry," APL Photonics **7**, 071101 (2022).
[28]W. Withayachumnankul, B. M. Fischer, and D. Abbott, "Material thickness optimisation for transmission-mode terahertz time-domain spectroscopy," Optics Express **16**, 7382 (2008).